nature communications

Article

https://doi.org/10.1038/s41467-026-68493-2

Targeting the UFL1-AKT cascade suppresses triple-negative breast cancer progression

Received: 13 March 2025

Accepted: 9 January 2026

Published online: 20 January 2026

Check for updates

Xiao Yang[1,2,9], Yalei Wen[2,9], Xiuqing Ma[2,9], Shengying Qin[3,4,9], Yixia Liu[2], Jiaqi Chen[2], Haoxing Zhang[5], Colin R. Goding[6], Rutao Cui[7,8] & Tongzheng Liu[1,2]

Triple-negative breast cancer (TNBC) is an aggressive and highly lethal disease with limited therapies. While UFL1-mediated UFMylation has been implicated in various diseases, its role in TNBC remains not fully understood. Here, we demonstrate that AKT1 directly interacts with UFL1 and undergoes UFMylation at Lys189/276/297. This modification enhances AKT phosphorylation and activation, promoting tumor growth and chemoresistance in TNBC. In turn, AKT phosphorylates UFL1 at Thr426, establishing a positive feedback loop that sustains high activity of both pro-oncogenic regulators in TNBC. Disrupting the UFL1-AKT interaction using the specific peptide PDAU-TAT significantly inhibits TNBC progression both in vitro and in vivo. Clinically, elevated pT426 UFL1 correlates with high pAKT in TNBC specimens. These findings uncover a crucial UFL1-AKT positive feedback loop that drives TNBC progression and suggest that targeting this axis could offer a promising therapeutic strategy for TNBC and potentially other aggressive cancers characterized by upregulated UFL1 and AKT activation.

Triple-negative breast cancer (TNBC) is the most aggressive subtype of breast cancer characterized by the absence of estrogen receptor (ER), progesterone receptor (PR) and human epidermal growth factor receptor-2 (HER2) expression[1]. The clinical management of TNBC is challenging due to the lack of targeted therapies. While standard chemotherapies such as cisplatin and paclitaxel are commonly used, their effectiveness is limited by the frequent development of chemoresistance and the higher metastatic potential of TNBC[2]. Therefore, there is an urgent need for novel targeted therapies that may significantly improve clinical outcomes for patients with TNBC.

UFMylation, a recently identified ubiquitin-like modification mediated by the E3 ligase UFL1, plays a crucial role in diverse cellular processes, including endoplasmic reticulum (ER) homeostasis[3,4], immunity[5,6], and DNA damage response[7,8]. Dysregulation of the UFMylation system has been associated with several diseases such as anemia and cancer[9–12]. Emerging evidence suggests that UFL1 can act either as a tumor suppressor or an oncogene, depending on the specific tumor context. For instance, UFL1 has been shown to ufmylate p53, thereby antagonizing MDM2-mediated ubiquitination, which stabilizes p53 and enhances its tumor-suppressive function in colorectal cancer[10]. Additionally, the loss of UFL1/UFBP1 in hepatocytes has been linked to liver carcinogenesis[13]. Conversely, UFL1-mediated UFMylation of the nuclear receptor coactivator ASC1 is crucial for ERα transactivation in response to 17β-estradiol, promoting ERα-mediated tumor formation in vivo[9]. Furthermore, UFMylation of ERα enhances its stability and transactivation, contributing to the development of ER$^+$ breast cancer[14]. However, despite these insights, the substrates of UFMylation and its precise biological functions in TNBC,

[1]Department of General Surgery, Guangzhou Red Cross Hospital of Jinan University, Guangzhou, China. [2]College of Pharmacy, Jinan University, Guangzhou, China. [3]Department of Oncology, The First Affiliated Hospital of Jinan University, Guangzhou, China. [4]Clinical Medical Research Institute, Jinan University, Guangzhou, China. [5]Guangdong Provincial Key Laboratory of Genome Stability and Disease Prevention, College of Life Sciences and Oceanography, Shenzhen University, Shenzhen, China. [6]Ludwig Institute for Cancer Research, University of Oxford, Headington, Oxford, UK. [7]Zhejiang University School of Medicine, Hangzhou, China. [8]FuRong Laboratory, Changsha, Hunan, China. [9]These authors contributed equally: Xiao Yang, Yalei Wen, Xiuqing Ma, Shengying Qin. e-mail: liutongzheng@jnu.edu.cn

the most malignant subtypes in breast cancer, remain poorly understood.

AKT, a key serine/threonine kinase, plays a crucial role in regulating various cellular processes, including cell growth, survival, metabolism, and proliferation[15,16]. In response to growth signals and stress stimuli, the pleckstrin homology (PH) domain of AKT binds to phosphatidylinositol (3,4,5)-trisphosphate (PIP3), enabling its membrane translocation[17]. At the membrane, AKT is phosphorylated by phosphoinositide-dependent kinase 1 (PDK1) at Thr308 and by mammalian target of rapamycin complex 2 (mTORC2) at Ser473, leading to its full activatation[18,19]. Activated AKT, in turn, phosphorylates numerous substrates, executing its effect on cellular processes[20,21]. AKT activation is tightly regulated through multiple mechanisms. The pleckstrin homology domain leucine-rich repeat protein phosphatases (PHLPP1/2) and protein phosphatase 2 A (PP2A) complex exert site-specific inhibition of AKT through dephosphorylation[20]. Specifically, PHLPP1/2 dephosphorylate AKT at SerS473[22,23], while PP2A targets Thr308 for dephosphorylation[24,25]. Additionally, phosphatase and tensin homolog (PTEN) and SH2 domain-containing inositol 5-phosphatase 1 (SHIP-1) dephosphorylate PIP3, thereby reducing AKT activation and negatively regulating this pathway[26,27]. However, mutations or amplifications in upstream components, such as the PI3K catalytic subunit (PIK3CA), mTOR complex components, oncogenic drivers like KRAS, receptor tyrosine kinases, and the loss of negative regulators like PTEN, can lead to increased PIP3 production, deregulated AKT activation, and enhanced tumor progression[28–31]. In TNBC, sustained aberrant AKT activation is frequently observed and plays a pivotal role in cell proliferation, apoptosis resistance, and metastasis, correlating with poor prognosis[32,33]. However, pathological mutations in key upstream regulators of AKT, such as PIK3CA[34,35], mTOR complex components[36], PTEN[35], and KRAS[37], are less frequent in TNBC compared to other breast cancer types. The mechanisms driving persistent AKT activation in TNBC remain poorly understood.

In this study, we present the initial evidence that AKT directly interacts with UFL1 and undergoes UFMylation in TNBC, a modification essential for AKT activation and its oncogenic functions. Furthermore, we show that AKT phosphorylates UFL1 at Thr426, establishing a positive feedback loop that sustains high activity of both pro-oncogenic regulators in TNBC. Disrupting UFL1-AKT interaction using the specific peptide PDAU-TAT significantly inhibits AKT activation and suppresses TNBC progression. Clinically, elevated levels of phosphorylated UFL1 (p-T426 UFL1) correlate with increased pAKT expression in TNBC specimens. Collectively, these findings reveal the critical role of the UFL1-AKT feedback loop in TNBC and suggest that targeting the UFL1-AKT1 axis may provide a promising therapeutic strategy for cancer treatment.

Results

UFL1 exerts an oncogenic role in TNBC

To investigate the role of UFL1 in TNBC, we analyzed data from The Cancer Genome Atlas (TCGA) and revealed a significant upregulation of *UFL1* expression in TNBC samples compared to normal breast tissues (Fig. 1a). Immunohistochemistry further validated the increased UFL1 protein levels in TNBC specimens (Fig. 1b). To explore the functional role of UFL1 in TNBC, we depleted UFL1 in TNBC cell lines, MDA-MB-231 and HCC1806, and found that UFL1 depletion markedly inhibited cell proliferation and enhanced sensitivity to chemotherapies (Fig. 1c–e). Similar effects were observed in ER^+ (MCF-7 and T47D) and $HER2^+$ (BT-474 and SK-BR-3) cells (Supplementary Fig. 1a–d), with comparable reductions in proliferation across distinct subtypes (Supplementary Fig. 1c). In vivo xenograft experiments also showed that UFL1 depletion significantly suppressed TNBC progression (Fig. 1f, g). In tumors from mice treated with saline or cisplatin, UFL1 depletion in HCC1806 cells significantly reduced Ki67 expression and increased cleaved PARP1 staining, with more pronounced effects observed in the cisplatin-treated group (Supplementary Fig. 1e). These findings underscore the clinical relevance of UFL1 as a promising therapeutic target to overcome chemoresistance in TNBC.

UFL1 promotes tumor progression in TNBC via AKT activation

Despite the growing body of evidence implicating UFL1-mediated UFMylation in cancer and other diseases, specific inhibitors targeting UFMylation are not yet available[38]. Thus, identifying UFL1 substrates and targeting the UFL1-mediated oncogenic pathways in TNBC holds promise as a potential therapeutic strategy for treating this aggressive malignancy. To identify potential TNBC-specific substrates of UFL1, we performed tandem affinity purification and mass spectrometry using MDA-MB-231 cells stably expressing Flag-S-UFL1. Intriguingly, both AKT1 and AKT2 were identified as potential interactors of UFL1 (Fig. 2a). Co-immunoprecipitation experiments confirmed the interaction between UFL1 and pan-AKT, and further validation in HCC1806 cells demonstrated the endogenous interaction between UFL1 and AKT1 (Fig. 2b). In vitro binding assays revealed that GST-AKT1, but not GST alone, directly interacted with recombinant His-UFL1, with relatively weaker interactions observed between UFL1 and AKT2/AKT3 (Fig. 2c). Immunofluorescence staining also showed co-localization of UFL1 with AKT1 in MDA-MB-231 cells (Supplementary Fig. 2a).

Given the central role of AKT in cellular processes such as cell proliferation and apoptosis, and its deregulation in various cancers[39], we next investigated whether UFL1 modulates AKT stability or activation in TNBC. As shown in Fig. 2d, UFL1 depletion in MDA-MB-231 and HCC1806 cells resulted in a significant decrease in AKT phosphorylation, as well as reduced phosphorylation of downstream targets GSK-3β and PRAS40, without affecting their total protein levels. These results were consistent across various breast cancer subtypes, including ER^+ (MCF-7 and T47D) and $HER2^+$ (BT-474 and SK-BR-3) breast cancer cell lines (Supplementary Fig. 2b), indicating that UFL1-driven AKT activation of AKT is a common regulatory mechanism in breast cancer. Conversely, overexpression of Flag-UFL1 enhanced the phosphorylation of AKT, GSK-3β and PRAS40 (Fig. 2e, Supplementary Fig. 2c). The pan-AKT inhibitor capivasertib markedly reduced phosphorylation of AKT downstream substrates in control TNBC cells, but this effect was attenuated in UFL1-overexpressing cells (Supplementary Fig. 2d). Consistently, capivasertib suppressed proliferation and enhanced sensitivity to cisplatin and doxorubicin, with weaker effects in UFL1-overexpressing cells (Fig. 2f, g). Together, these results collectively suggest that UFL1 promotes TNBC progression through AKT activation.

UFL1 ufmylates AKT1 at Lys189, Lys276, and Lys297

As UFL1 functions as the E3 ligase responsible for UFMylation, we examined whether UFL1 modifies AKT through this mechanism. In cells co-transfected with UFMylation machinery components, including UBA5, UFC1, UFL1, UFM1 ΔC2 (an active form of UFM1) and UFBP1, UFMylation signal was detected in AKT1 immunoprecipitates, as evidenced by a 20kDa shift compared to unmodified AKT1 (Fig. 3a). Similar results were observed in an in vitro UFMylation assay (Fig. 3b). UFMylation of endogenous AKT1 was also observed in MDA-MB-231 and HCC1806, and this modification was significantly reduced upon UFL1 depletion (Fig. 3c).

To map the UFMylation sites on AKT1, we identified that the N-terminal region of UFL1 (amino acids 1–247) interacts with AKT1 (Fig. 3d, e). Further analysis revealed that the kinase domain of AKT1 (amino acids 148–410) is responsible for this (Fig. 3f, g). Additionally, UFMylation was present on the full-length AKT1 and the kinase domain (amino acids 148-410) (Fig. 3h). To define the potential UFMylation sites on AKT1, we constructed six mutants (K154R, K189R, K276R, K284R, K297R and K377R) within the kinase domain, based on potential ubiquitination sites predicted by the PhosphoSitePlus database. Single mutations at K189R, K276R, or K297R partially reduced

https://doi.org/10.1038/s41467-026-68493-2

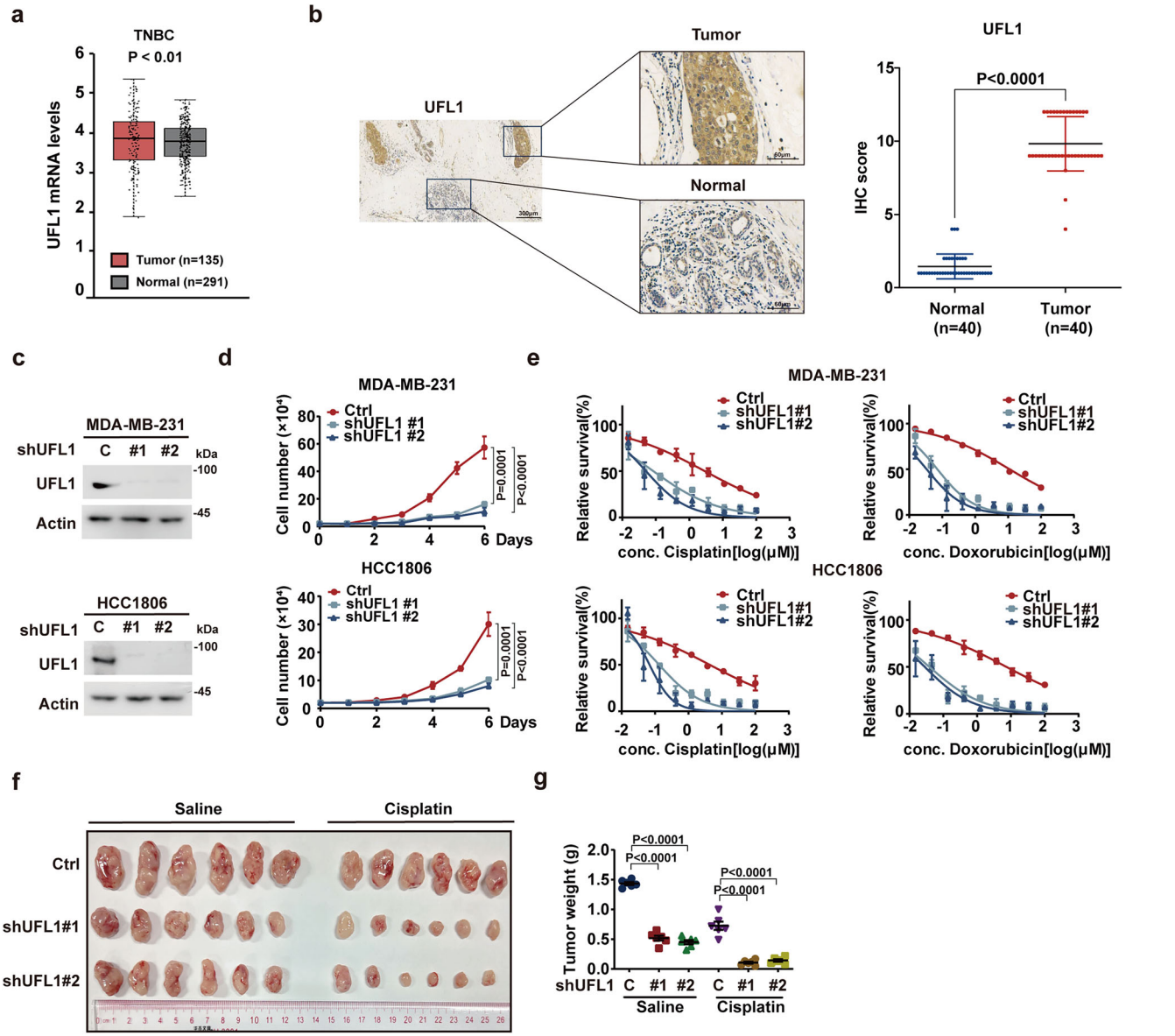

Fig. 1 | UFL1 exerts an oncogenic role in TNBC. a *UFL1* mRNA expression level in TNBC ($n = 135$) and normal breast tissues ($n = 291$) was analyzed via the GEPIA database ($P < 0.01$). In the box plot, the upper and lower whiskers represent the maximum and minimum values, respectively. The upper and lower boundaries of the box correspond to the upper and lower quartiles, and the line within the box indicates the median. **b** Representative immunohistochemical (IHC) staining and scores of UFL1 in TNBC and adjacent normal tissues ($n = 40$). The left panel displayed a low-magnification field of view (scale bar, 300 μm); the right panels were magnified views of the boxed regions (scale bar, 60 μm). **c** MDA-MB-231 and HCC1806 cells stably expressing control or UFL1 shRNAs were analyzed by Western blotting. **d** Cell proliferation of cells in (**c**) was examined. **e** Cells as in (**c**) were treated with the indicated concentrations of cisplatin or doxorubicin, and cell survival was determined. **f**, **g** HCC1806 cells in (**c**) were subcutaneously implanted into nude mice. Mice were treated with saline or cisplatin (5 mg/kg weekly, $n = 6$) when tumor volume reached 100 mm^3. Tumors were collected (**f**), and tumor weights were measured (**g**) (means ± SD). Western blotting is representative of three independent experiments (**c**). Data were presented as mean ± SD of three independent experiments (**d**, **e**). Data were analyzed by two-sided one-way ANOVA in (**d**, **g**), by *t*-test in (**a**, **b**). Source data are provided as a Source Data file.

AKT1 UFMylation (Supplementary Fig. 3a), whereas K284R, K377R, or those in PH domain (K14R, K20R, K30R or K64R) had little effect on AKT1 UFMylation (Supplementary Fig. 3a, b). Notably, simultaneous mutation of K189R, K276R, and K297R (3KR) almost completely abolished AKT1 UFMylation across HEK293T, TNBC (MDA-MB-231 and HCC1806), ER^+ (MCF-7 and T47D) and $HER2^+$ (BT474 and SK-BR-3) cells (Fig. 3i, j, Supplementary Fig. 3c–g), indicating conserved AKT1 UFMylation at Lys189, Lys276, and Lys297.

UFL1-mediated UFMylation is critical to activate AKT in TNBC

Upon insulin stimulation, AKT1 UFMylation peaked at 15 min, preceding maximal Ser473 phosphorylation (Supplementary Fig. 4a), suggesting a priming role of UFMylation. Disrupting AKT1 UFMylation, either by UFL1 depletion or reconstituting the AKT1 3KR mutant in endogenous AKT1/2/3-deficient cells, did not alter AKT recruitment to the cell membrane (Supplementary Fig. 4b–d). This observation led us to hypothesize that UFMylation might regulate AKT phosphorylation by affecting its interaction with specific kinases or phosphatases. As shown in Fig. 4a and Supplementary Fig. 4e, the AKT1 3KR mutant impaired interaction with mTOR and Rictor (two key components of mTORC2[40]) but not with PHLPP1, a phosphatase that selectively dephosphorylates AKT at Ser473[23]. Far-western assays using in vitro UFMylated GST-AKT1 showed stronger binding to purified Flag-mTOR compared with the unmodified protein (Supplementary Fig. 4f, g).

https://doi.org/10.1038/s41467-026-68493-2

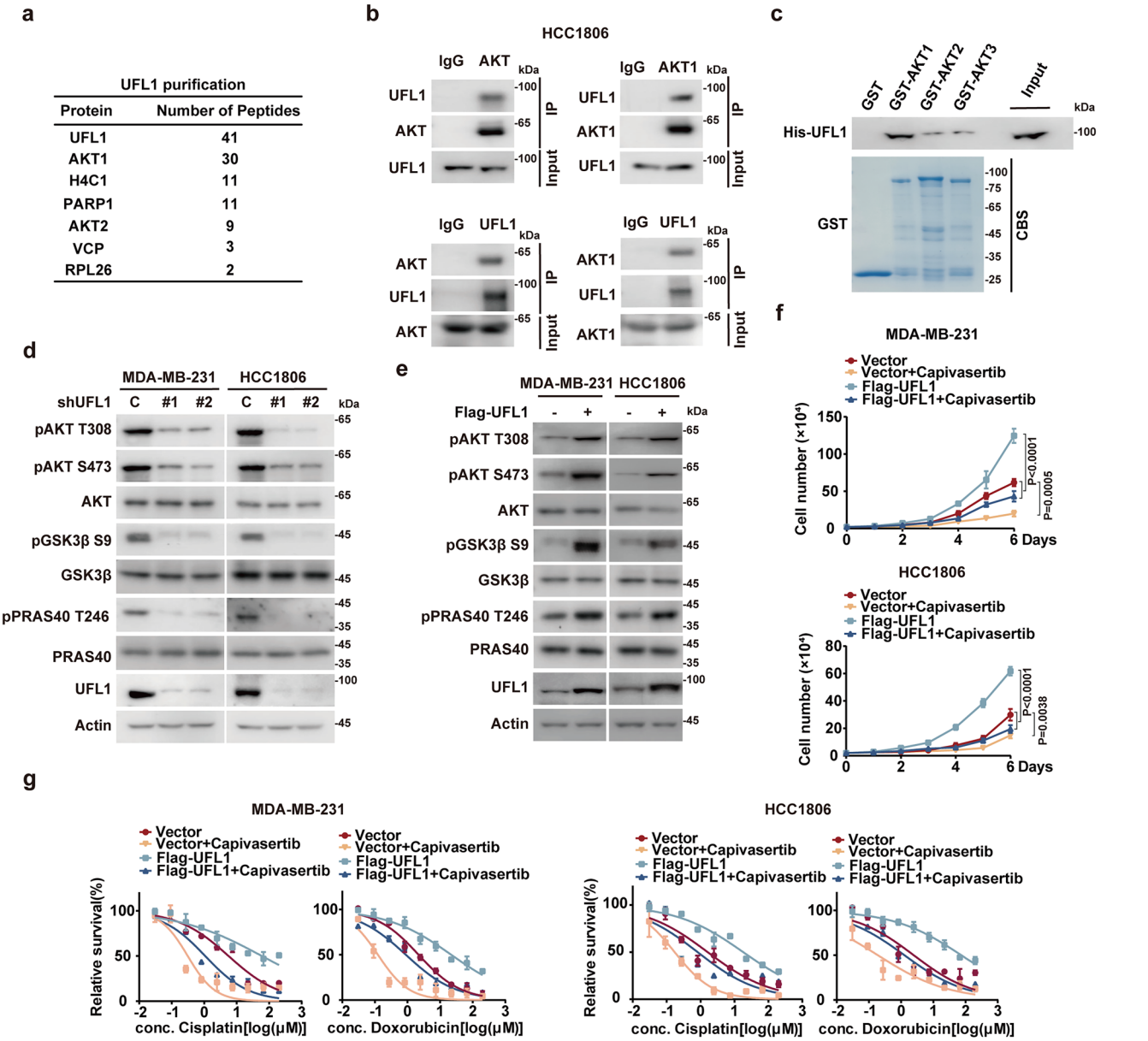

Fig. 2 | UFL1 promotes TNBC progression via AKT activation. a List of UFL1-associated proteins identified by mass spectrometric analysis. MDA-MB-231 cells stably expressing Flag-S-UFL1 were treated with MG132 (10 μM) for 10 h. UFL1 immunoprecipitates were subjected to mass spectrometric analysis ($n = 3$). **b** Endogenous co-immunoprecipitation confirms UFL1-AKT interaction. **c** Purified GST, GST-AKT1/2/3 and His-UFL1 were incubated in vitro as indicated. The interaction between UFL1 and AKT1/2/3 was examined. CBS, Coomassie blue staining. **d** Western blotting of MDA-MB-231 and HCC1806 cells stably expressing control or UFL1 shRNAs using the indicated antibodies. **e** Western blotting of cells stably expressing empty vector or Flag-UFL1 using the indicated antibodies. **f** Cells as in (**e**) were treated with vehicle or capivasertib, and a cell proliferation assay was performed. **g** Cells as in (**f**) were treated with DMSO or indicated concentrations of cisplatin or doxorubicin, and cell survival was determined. Mass spectrometric analysis and western blotting are representative of three independent experiments (**a**, **d**, **e**). Data were presented as mean ± SD of three independent experiments (**f**, **g**). Data were analyzed by two-sided one-way ANOVA in (**f**). Source data are provided as a Source Data file.

Conversely, the AKT1 3KR mutant exhibited increased interaction with PP2A B55α, which promotes Thr308 dephosphorylation[41], without altering interaction with PDK1 or PP2A B56β, both critical regulators of AKT Thr308 phosphorylation[24,42] (Fig. 4b, Supplementary Fig. 4h). Similar changes were observed upon UFL1 depletion in HCC1806 cells (Supplementary Fig. 4i, j). Further AKT1/SIN1 structural modeling suggested UFM1 conjugated via its terminal Gly83 to K189 of AKT1 establishes stabilizing contacts with AKT1 residues Phe237 and Arg241 and SIN1 residues Asp237 and Ser260, creating an auxiliary interface that enhances mTORC2 recruitment (Supplementary Fig. 4k). Moreover, AKT1/B55α structural modeling implicated Lys189/Lys276/Lys297 in the interface and UFMylation at these residues is predicted to introduce substantial steric hindrance that weakens B55α binding (Supplementary Fig. 4l). Together, these findings indicate that UFMylation promotes AKT1 phosphorylation by enhancing mTORC2 recruitment and restricting PP2A B55α binding.

To assess the reversibility of UFMylation, we depleted the UFM1-specific protease UFSP2. As shown in Supplementary Fig. 5a, loss of UFSP2 caused marked accumulation of UFMylated AKT1 in control and UFMylation machinery-transfected MDA-MB-231 cells, enabling detection of UFMylated AKT1 by Flag or AKT1 immunoblotting (Supplementary Fig. 5b, c). Under UFSP2 knockdown, UFL1 overexpression markedly induced a shifted p-AKT band co-migrating with UFMylated AKT1, and UFMylated p-AKT S473 was detectable (Supplementary

https://doi.org/10.1038/s41467-026-68493-2

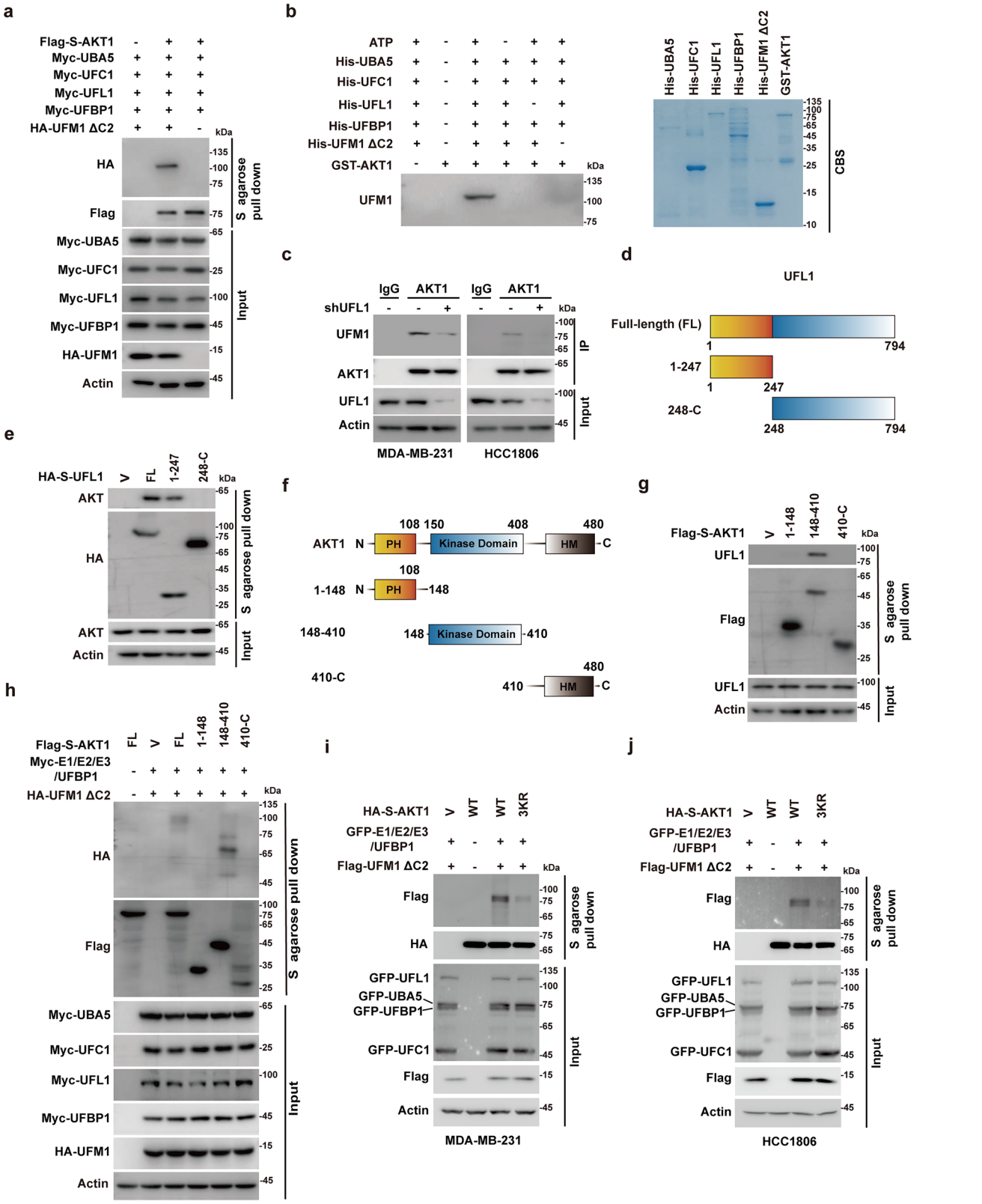

Fig. 5d, e). Notably, UFSP2 preferentially bound active AKT1 mutants (T308D, S473D or T308D/S473D) over inactive forms (T308A, S473A or T308A/S473A)[43] (Supplementary Fig. 5f), suggesting that UFMylation is rapidly removed following AKT phosphorylated. Such transient cycles of UFMylation and de-UFMylation are likely required for substrate engagement, given that all UFMylation sites Lys189, Lys276 and Lys297 lie within the AKT1 catalytic domain.

To examine the biological consequences of UFL1-mediated UFMylation of AKT1 in TNBC, we reconstituted AKT1 WT or the AKT1 3KR mutant in AKT1/2/3-deficient HCC1806 and MDA-MB-231 cells. Compared to AKT1 WT, the AKT1 3KR mutation significantly reduced AKT activation (Fig. 4c and Supplementary Fig. 5g). Reconstitution of AKT1 WT, but not the 3KR mutant, in AKT1/2/3-deficient HCC1806 and MDA-MB-231 cells significantly promoted cell proliferation and

Fig. 3 | UFL1 ufmylates AKT1 at Lys189, Lys276, and Lys297. a In vivo UFMylation assay of AKT1 in HEK293T cells transfected with Flag-S-AKT1 and the components of the UFMylation system. **b** In vitro UFMylation assay of AKT1. Samples were subjected to western blotting with an anti-UFM1 antibody. **c** In MDA-MB-231 and HCC1806 cells stably expressing control or UFL1 shRNA, UFMylation of endogenous AKT1 was detected by immunoprecipitation with an anti-AKT1 antibody, followed by subsequent western blotting using an anti-UFM1 antibody. **d** A schematic showing the generation of the UFL1 full-length (FL), 1–247 aa and 248-C aa constructs. **e** Cells were transfected with vector, HA-S-UFL1 full length or HA-S-UFL1 truncation mutants (1–247 aa and 248-C aa). Cell lysates were pulled down using S-agarose, and the interaction between UFL1 and AKT1 was then examined. **f** A schematic showing the generation of the AKT1 full-length (FL), 1–148 aa, 148–410 aa and 410–C aa constructs. **g** Cells were transfected with vector, Flag-S-AKT1 truncation mutants (1–148, 148–410 and 410-C). Cell lysates were pulled down using S-agarose, and the interaction between UFL1 and AKT1 was then examined. **h** UFMylation assay of the Flag-S-AKT1 full length and its truncation mutants (1–148 aa, 148–410 aa or 410-C aa) was examined in HEK293T cells. **i**, **j** UFMylation assay of the HA-S-AKT1 WT and 3KR was performed in MDA-MB-231 and HCC1806 cells. Source data are provided as a Source Data file.

decreased cellular sensitivity to cisplatin and doxorubicin in vitro and in vivo (Fig. 4c–f, Supplementary Fig. 5g, h). In HCC1806 cells, reconstitution of AKT1 WT, but not the 3KR mutant, dramatically enhanced cell proliferation as indicated by Ki67 staining, and reduced apoptosis as shown by decreased cleaved PARP1 staining (Fig. 4g). These results demonstrate that UFL1-mediated UFMylation is critical for AKT activation and enhances its oncogenic function in TNBC.

AKT phosphorylates UFL1 at the T426 site to enhance its UFMylation and promote TNBC progression

Surprisingly, we observe a dose-dependent decrease in AKT UFMylation following treatment with capivasertib (Fig. 5a), suggesting that AKT inhibition may impair its UFMylation. This led us to hypothesize that activated AKT may phosphorylate UFL1, which in turn could modulate AKT UFMylation. To test this hypothesis, we assessed the phosphorylation of overexpressed Flag-S-UFL1 in HCC1806 cells using a phospho-AKT substrate antibody (Fig. 5b). Inhibition of AKT activity reduced UFL1 phosphorylation (Fig. 5c). Further investigation revealed a conserved phosphorylation site at Thr426 within the UFL1 amino acid sequence. This site is highly conserved across species and aligns with the AKT consensus phosphorylation motif (RXRXXS*/T*) (Fig. 5d). A phospho-Thr426-specific antibody was generated to study the phosphorylation of UFL1 at this site in cells. As shown in Fig. 4e, the phosphorylation-deficient T426A mutant almost completely abolished UFL1 phosphorylation. Treatment with capivasertib or depletion of AKT1/2/3 significantly reduced UFL1 phosphorylation at T426 (pUFL1 T426) (Fig. 5f, g). Functionally, the T426A mutant impaired AKT1 UFMylation (Fig. 5h) and decreased UFMylation of two established substrates, RPL26 and ERα[9,44](Supplementary Fig. 6a, b). Moreover, during the revision of this work, an independent study reported AKT-dependent UFL1 phosphorylation at T426 promoting UFMylation of ArPC4 and lung cancer metastasis[45], consistent with our findings.

Mechanistically, the T426A mutation or capivasertib treatment significantly reduced UFL1 binding to UFBP1 and CDK5RAP3 without affecting UFC1 interaction (Fig. 5i, j). T426 is located within the peptidyl transferase center (PTC) loop, implicated in UFMylation complex assembly[44]. We therefore propose that phosphorylation at this site may induce conformational changes that promote UFBP1/CKD5RAP3 recruitment, thereby enhancing UFL1 enzymatic activity.

We then examined the biological function of UFL1 phosphorylation in TNBC. Overexpression of Flag-UFL1 WT, but not the T426A mutant, increased phosphorylation of AKT, GSK-3β and PRAS40 in HCC1806 and MDA-MB-231 cells (Fig. 5k, Supplementary Fig. 6c). UFL1 WT also significantly enhanced cell proliferation and reduced sensitivity to cisplatin and doxorubicin, while the T426A mutant did not (Fig. 5k, l, Supplementary Fig. 6c, d). These results demonstrate that UFL1 phosphorylation at Thr426 plays a crucial role in maintaining AKT activation and enhancing the oncogenic function of both UFL1 and AKT in TNBC.

Disrupting the UFL1-AKT1 interaction suppresses TNBC progression

Given the positive feedback loop between UFL1 and AKT in TNBC, we hypothesized that disrupting their interaction could inhibit AKT activation and suppress tumor progression. To identify the minimal region of UFL1 responsible for binding to AKT1, we tested truncated UFL1 protein fragments and identified amino acids 20–30 as critical for binding to AKT1, both in vivo and in vitro (Fig. 6a, b).

Cell-penetrating peptides have gained attention as promising tools to target specific molecular pathway[46,47]. To disrupt the UFL1-AKT interaction, we synthesized a peptide corresponding to UFL1 amino acids 20–30, as well as a negative control peptide corresponding to amino acids 1–10. Both peptides were conjugated to the TAT peptide (GRKKRRQRRRGG) to form cell-penetrating peptides termed PDAU (Peptide Disrupting AKT-UFL1 interaction) and NP (negative peptide), respectively (Fig. 6c). Isothermal titration calorimetry (ITC) confirmed direct binding of PDAU to AKT1 with K_d values of 25.9 μM, comparable to wild-type UFL1 (17.6 μM), whereas NP showed no detectable binding (Supplementary Fig. 7a). Pharmacokinetic analysis demonstrated a mean half-life of 1.29 ± 0.15 h following intravenous (IV) administration and 3.74 ± 0.94 h following intraperitoneal (IP) administration (Table S1, S2, Supplementary Fig. 7b). In vivo imaging with Cy5-labeled PDAU in tumor-bearing mice revealed peak accumulation at 8 h, with widespread distribution and progressive clearance within 24 h, leaving low residual signal in tumor and liver (Supplementary Fig. 7c, d).

We next assessed the ability of these peptides to disrupt the UFL1-AKT interaction in HCC1806 cells. As shown in Fig. 6d, PDAU, but not NP, effectively interfered with the UFL1-AKT binding. Consistently, PDAU reduced AKT UFMylation and suppressed AKT phosphorylation across diverse breast cancer subtypes (Fig. 6e, f, Supplementary Fig. 7e), while NP had no such effect. Functionally, PDAU treatment significantly inhibited cell proliferation and sensitized breast cancer cells to chemotherapies (Fig. 6g, h). PDAU also decreased UFL1 phosphorylation at T426, while causing only modest changes in global UFMylation (Supplementary Fig. 7f), suggesting that PDAU preferentially modulates the UFMylation of certain substrates rather than exerting a broad effect on the global UFMylation landscape.

We further validated the therapeutic potential of PDAU in cancer cell line-derived xenograft (CDX) and patient-derived xenograft (PDX) models (Fig. 7a, b, Supplementary Fig. 8a). In the PDX model, PDAU treatment significantly disrupted the UFL1-AKT interaction and inhibited AKT phosphorylation in tumor samples (Fig. 7c, d). Consistent with these effects, PDAU markedly decreased Ki67 expression and increased cleaved PARP1 staining in cisplatin-treated PDX tumors (Fig. 7e). Importantly, PDAU treatment did not induce liver or kidney toxicity (Supplementary Fig. 8b), nor did it affect the body weight (Supplementary Fig. 8c). H&E staining also showed no apparent damage to major organs, including the heart, liver, spleen, lung and kidney (Supplementary Fig. 8d). In TNBC xenografts, PDAU produced stronger tumor growth inhibition than capivasertib (Supplementary Fig. 8e). In contrast, in non-tumorigenic MCF 10A cells, PDAU caused weaker reduction of AKT substrate phosphorylation (GSK3β Ser9 and PRAS40 Thr246) compared with capivasertib (Supplementary Fig. 8f). UFL1 protein levels were lower in MCF 10A cells than diverse breast cancer cells (Supplementary Fig. 8g), which may account for PDAU's reduced effect in normal cells and suggest an improved therapeutic window. Together, these findings demonstrate that PDAU disrupts the UFL1-AKT interaction to inhibit AKT activation and breast cancer

https://doi.org/10.1038/s41467-026-68493-2

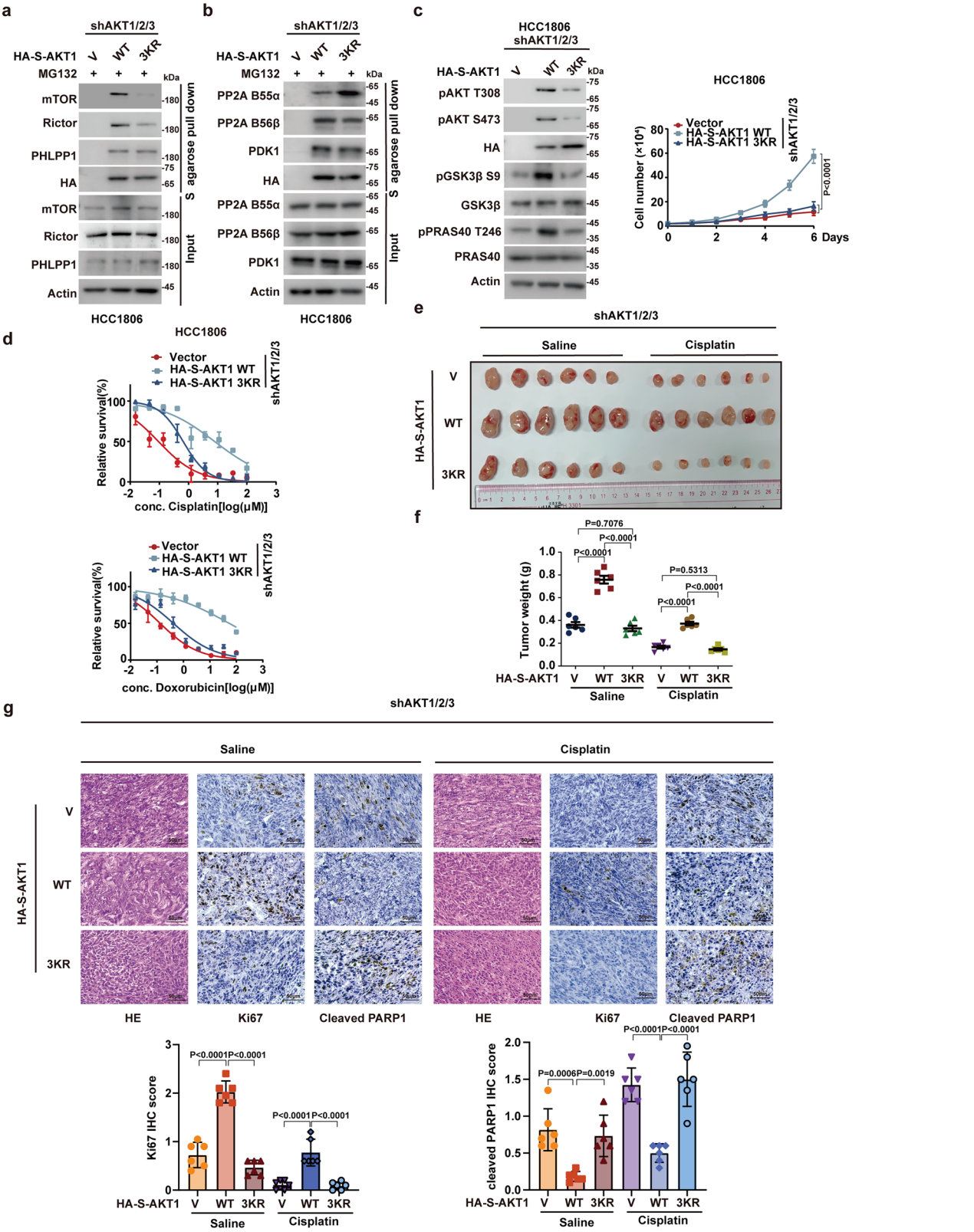

progression while sparing normal tissues, highlighting its therapeutic potential.

Correlations between pUFL1 and pAKT expression in TNBC

To further explore the clinical relevance of the UFL1-AKT positive feedback loop, we analyzed expressions of pUFL1 and pAKT in TNBC specimens ($n = 40$) using immunohistochemistry. As shown in Fig. 8a–c, the expressions of pUFL1 were positively correlated with pAKT levels in TNBC specimens. Collectively, our findings underscore the critical role of UFL1-mediated UFMylation of AKT in TNBC progression, and suggest that targeting the UFL1-AKT axis, particularly by disrupting their interaction, could provide a promising therapeutic strategy for TNBC, and potentially other aggressive cancers with

Fig. 4 | UFL1-mediated UFMylation is critical to activate AKT in TNBC. a, **b** HCC1806 cells were transfected with the indicated plasmids and treated with MG132 for 10 h before harvest. Cell lysates were pulled down using S-agarose, and the interaction between AKT1 and the indicated proteins was then examined. **c** AKT1/2/3-depleted HCC1806 cells were transfected with the indicated plasmids, and western blotting was performed as indicated. Cell proliferation was measured. **d** Cells as in (c) were treated with the indicated concentrations of cisplatin or doxorubicin, and cell survival was determined. **e**, **f** Nude mice were subcutaneously inoculated with HCC1806 cells (2×10^6) stably expressing either an empty vector, HA-S-AKT1 WT, or the 3KR mutant. Treatment with saline or cisplatin (5 mg/kg, once weekly) commenced when the xenograft tumors reached approximately 100 mm^3 ($n = 6$ per group). Tumors were subsequently harvested (**e**) and weighed (**f**). Data are presented as the mean ± SD for each group of six mice. **g** IHC staining and quantification of Ki67 and cleaved PARP1 expression in a subcutaneous tumor model ($n = 6$) from (**e**). Scale bars, 50 μm. Data are shown as means ± SD. Western blotting is representative of three independent experiments (**c**). Data were presented as mean ± SD of three independent experiments (**c**, **d**). Data were analyzed by two-sided one-way ANOVA in (**c**, **f**, **g**). Source data are provided as a Source Data file.

aberrantly elevated UFL1 expression and hyperactivation of AKT (Fig. 8d).

Discussion

In this study, we identify a previously overlooked oncogenic role of UFL1-mediated UFMylation in sustaining AKT activation and driving TNBC progression. We show that UFL1 directly interacts with AKT1 and catalyzes UFMylation at Lys189, Lys276, and Lys297. Unlike other post-translational modifications, such as TRAF6 and Skp2-mediated ubiquitination at Lys8 and Lys14, or PRMT5-mediated methylation at Arg15 and Arg391[48–50], which regulate AKT membrane translocation, UFMylation occurs within the catalytic domain. This modification provides a distinct regulatory layer by facilitating AKT1 interaction with mTORC2 and disrupting its association with PP2A B55α, thereby enhancing phosphorylating at S473 and T308 and sustaining AKT activation. Genetic depletion of UFL1 or expression of UFMylation-deficient AKT mutants impairs AKT phosphorylation and oncogenic function, establishing UFMylation as a critical regulatory mechanism for AKT signaling. Moreover, UFMylaion proved to be dynamic, with UFSP2 preferentially binding to active AKT1 mutants and rapidly removing the modification, suggesting that UFMylation in the catalytic domain primes AKT1 phosphorylation but is removed once phosphorylation occurs, potentially to ensure accessibility of AKT to downstream substrates.

We further reveal a reciprocal feedback loop between UFL1 and AKT. AKT phosphorylates UFL1 at Thr426, a residue within the peptidyl transferase center (PTC) loop, implicating UFMylation machinery assembly[44]. Phosphorylation at Thr426 enhanced UFL1 interaction with UFBP1 and CDK5RAP3 (Fig. 5i, j), thereby stimulating enzymatic activity and broadening substrate UFMylation, including AKT1, RPL26, ERα (Fig. 5, Supplementary Fig. 6a, b), as well as AsPC4[45]. These findings, supported by the positive correlation between p-T426 UFL1 and p-AKT levels in TNBC samples (Fig. 8), suggest that Thr426 phosphorylation may function as a conformational switch that sustains UFMylation and AKT activation. Although direct structural evidence is lacking, this feedback loop likely amplifies oncogenic signaling and warrants further biochemical and structural investigation.

Our findings also clarify the tumor-context-dependent role of UFL1. While downregulated in melanoma and hepatocellular carcinoma[51], UFL1 is markedly upregulated in ERα-positive breast cancer, where it promotes tumorigenesis through UFMylating ASC1 and ERα[9,14]. Here, we show that UFL1 is markedly elevated in TNBC at both transcript and protein levels (Fig. 1a, b). This elevated expression likely contributes to persistent AKT activation and aggressive phenotypes. The upstream regulation of UFL1 in TNBC remains poorly understood, though evidence from glioblastoma implicates non-coding RNAs such as HSD52 in stabilizing UFL1 mRNA[52]. Additionally, kinases such as ATM and AMPK phosphorylate UFL1 under various stress conditions[6,8]. These findings highlight multilayered mechanisms governing UFL1 expression and activity.

Therapeutically, we establish proof-of-concept for disrupting the UFL1-AKT axis using the cell-penetrating peptide PDAU. Although direct AKT inhibitors, including capivasertib, have entered clinical use, their benefit is often constrained by toxicity, limited selectivity, acquired resistance, and the absence of predictive biomarkers[53,54]. Consistent with their broad physiological role, AKT inhibitors are frequently associated with adverse effects such as diarrhea, rash, and hyperglycemia in clinical studies[55–57]. Here, our study demonstrates that PDAU effectively inhibits AKT activation (Fig. 6f, Supplementary Fig. 7e), suppresses TNBC progression in CDX and PDX models (Fig. 7a, b, Supplementary Fig. 8a), and enhances chemosensitivity to cisplatin and doxorubicin (Fig. 6h). Importantly, PDAU treatment was well tolerated, with no significant changes in body weight or histopathological abnormalities in major organs in treated mice (Supplementary Fig. 8b–d). Compared with capivasertib, PDAU elicited stronger tumor growth inhibition while exerting weaker effects on AKT signaling in non-tumorigenic MCF 10A breast epithelial cells (Supplementary Fig. 8e, f), reflecting improved tumor selectivity. This selectivity likely reflects the lower UFL1 expression in MCF 10A cells and normal breast tissues relative to TNBC (Fig. 1a, b, Supplementary Fig. 8g), indicating that PDAU preferentially targets tumors with UFL1 upregulation and thus provides a favorable therapeutic window. Although the affinity of PDAU for AKT1 is modest, this is consistent with its nature as an unoptimized linear peptide. Linear peptides derived directly from protein–protein interaction interfaces typically display micromolar affinities, as they capture only part of the binding surface and lack conformational constraints[58,59]. Future optimization strategies such as cyclization, hydrocarbon stapling, and D-amino acid substitution are expected to improve affinity and stability[60]. In parallel, comprehensive pharmacological studies, including biodistribution, long-term toxicity, and immunogenicity, will be essential to refine the safety profile of PDAU and its derivative peptides and to enable their translational development.

Although our study focuses on TNBC, we also demonstrate that UFL1 regulates AKT activation in HR^+ and $HER2^+$ breast cancer models (Supplementary Fig. 2b, c, Supplementary Fig. 7e), suggesting broader relevance across breast cancer subtypes. Future studies should explore whether this axis contributes to AKT hyperactivation in other malignancies and assess its value as a predictive biomarker for therapeutic response.

In summary, we define a UFMylation-dependent mechanism that sustains AKT activation through a positive feedback loop with UFL1. By disrupting this interaction with PDAU, we provide mechanistic insight and preclinical evidence for targeting the UFL1-AKT axis as a therapeutic strategy in TNBC and potentially other cancers characterized by UFL1 upregulation and persistent AKT activation.

Methods

Ethical statement

This research complies with all relevant ethical regulations. All animal experiments were conducted in accordance with the protocols approved by the Institutional Animal Care and Use Committee of Jinan University. The experiment using patients' samples was approved by the Institutional Research Ethics Committee of Jinan University.

Cell culture, plasmids and antibodies

Cell lines HEK293T, MCF 10A, MDA-MB-231, HCC1806, MCF-7, T47D, BT-474 and SK-BR-3 cells were purchased from ATCC (American Type

https://doi.org/10.1038/s41467-026-68493-2

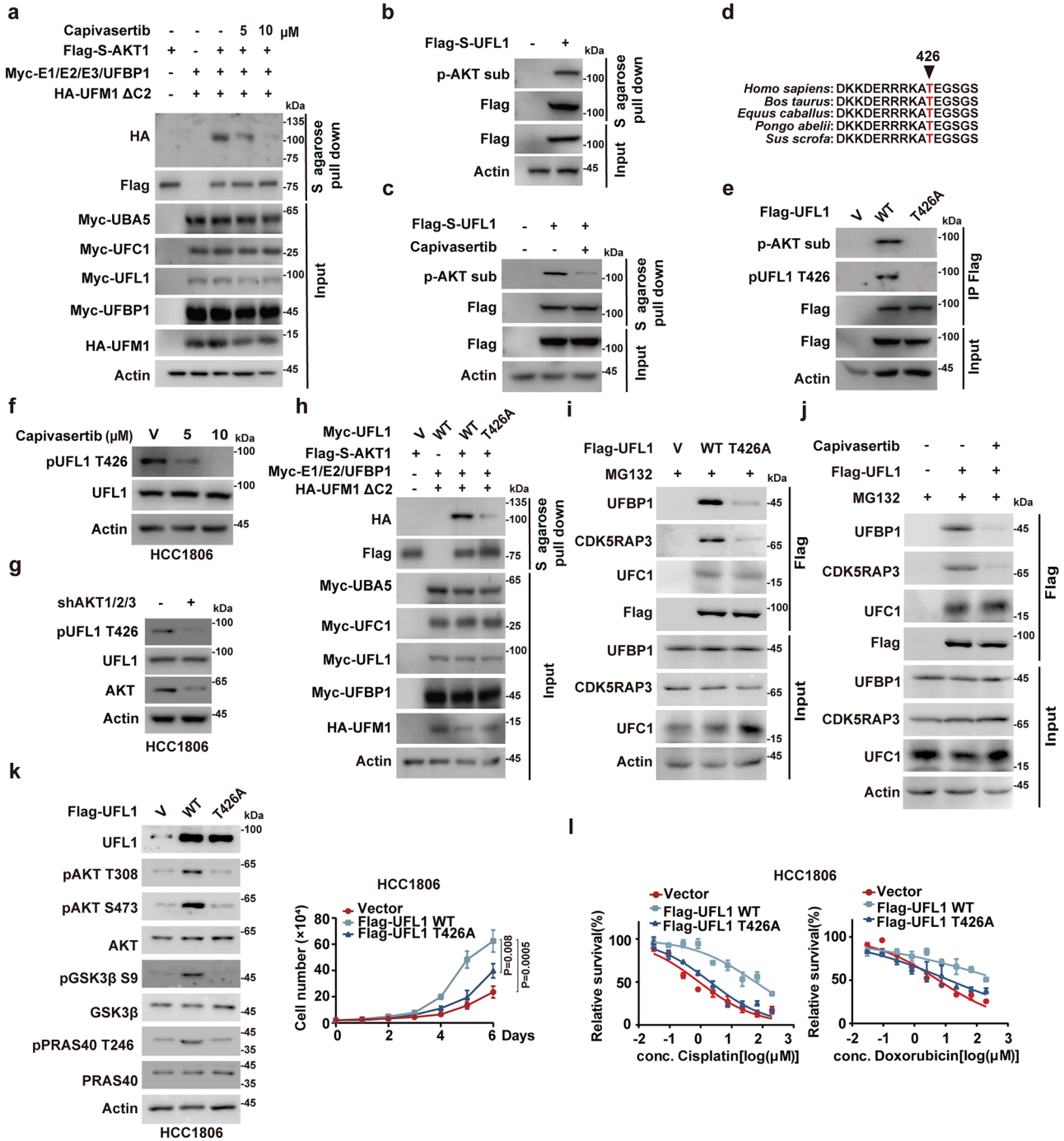

Fig. 5 | AKT phosphorylates UFL1 at the T426 site to enhance its UFMylation and promote TNBC progression. a UFMylation assay of the Flag-S-AKT1 was examined in cells treated with indicated concentrations of capivasertib. **b** Cells were transfected with vector or Flag-S-UFL1, followed by S-agarose pull-down. Western blotting was performed using the indicated antibodies. **c** Cells were transfected as indicated and treated with capivasertib (10 μM) for 24 h before harvest. Then, cell lysates were pulled down using S-agarose and western blotting was performed. **d** AA sequences around the T426 residue in UFL1 are conserved across different species. Arrows, threonine residues that are conserved across species. **e** Cells were transfected with vector, Flag-UFL1 WT or T426A mutant and cell lysates were subjected to immunoprecipitation with an anti-Flag antibody. Western blotting was performed using the indicated antibodies. **f** HCC1806 cells were treated with vehicle or indicated concentrations of capivasertib for 24 h, and western blotting was performed. **g** HCC1806 cells stably expressing control or AKT1/2/3 shRNAs were generated, and western blotting was performed using the indicated antibodies. **h** UFMylation assay of the Flag-S-AKT1 was examined in cells co-transfected with the indicated UFMylation system components. **i** Cells transfected as indicated were treated with MG132 and subjected to anti-Flag immunoprecipitation to assess UFL1 interaction with UFBP1, CDK5RAP3, or UFC1. **j** Cells were transfected with vector or Flag-UFL1 and treated with capivasertib (10 μM) for 24 h before harvest. Cell lysates were subjected to immunoprecipitation with an anti-Flag antibody. Western blotting was performed using the indicated antibodies. **k** HCC1806 cells stably expressing vector, Flag-UFL1 WT, or T426A mutant were generated, and western blotting was performed with the indicated antibodies. Cell proliferation was measured. **l** HCC1806 cells, as in (**k**), were treated with the indicated concentrations of cisplatin or doxorubicin and cell survival was determined. Western blotting is representative of three independent experiments (**f**, **g**, **k**). Data were presented as mean ± SD of three independent experiments (**k**, **l**). Data were analyzed by two-sided one-way ANOVA in (**k**). Source data are provided as a Source Data file.

https://doi.org/10.1038/s41467-026-68493-2

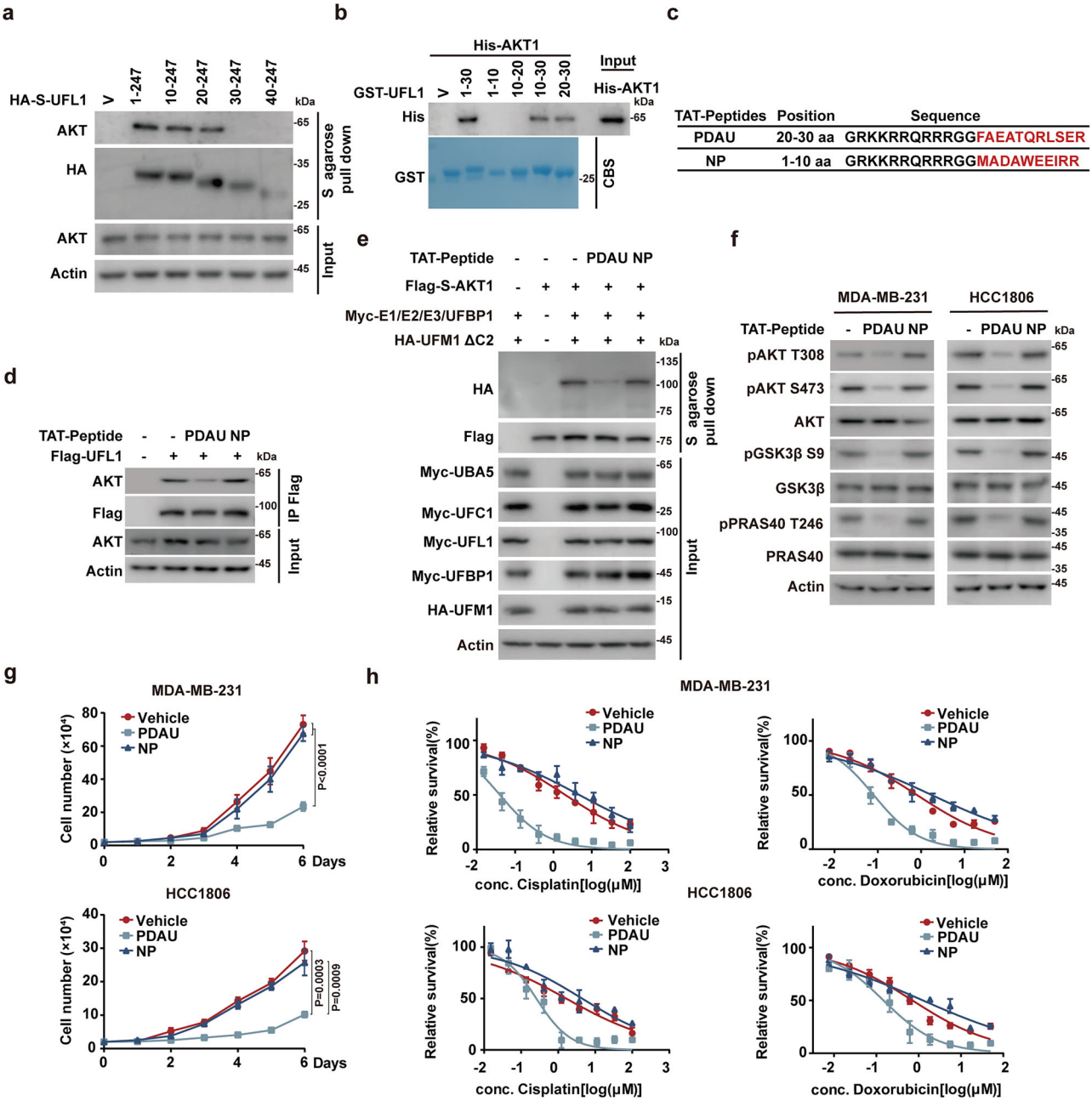

Fig. 6 | Disrupting the UFL1-AKT1 interaction by PDAU suppresses TNBC progression in vitro. a Cells transfected with vector, HA-S-UFL1 truncation mutants (1–247, 10–247, 20–247, 30–247, 40–247) were pulled down using S-agarose, and the interaction between UFL1 and AKT1 was then examined. **b** Purified recombinant GST, GST-UFL1 truncation mutants were incubated with purified His-AKT1 in vitro to assess the interaction between UFL1 and AKT1. **c** Two TAT-Peptides, PDAU (20-30 aa) and NP (1-10 aa), from UFL1 are shown. **d** Cells transfected as indicated were treated with vehicle (ddH_2O), PDAU or NP (10 μM) for 24 h before harvest and subjected to anti-Flag immunoprecipitation to assess UFL1 interaction with AKT. **e** UFMylation assay of Flag-S-AKT1 was performed in HEK293T cells treated with vehicle (ddH_2O), PDAU or NP (10 μM). **f** MDA-MB-231 and HCC1806 cells were treated with vehicle (ddH_2O), PDAU or NP (10 μM) for 24 h and western blotting was performed indicated antibodies. **g** Cell proliferation assay was performed from cells in (**f**). **h** Cells as in (**f**) were treated with the indicated concentrations of cisplatin or doxorubicin, and cell survival was determined. Western blotting is representative of three independent experiments (**f**). Data were presented as mean ± SD of three independent experiments (**g**, **h**). Data were analyzed by two-sided one-way ANOVA in (**g**). Source data are provided as a Source Data file.

Culture Collection). HEK293T, MDA-MB-231, MCF-7 and BT-474 cells were cultured in Dulbecco's Modified Eagle's medium (Gibco) supplemented with 10% FBS (Gibco). HCC1806 and T47D cells were cultured in RPMI-1640 medium (Gibco) supplemented with 10% FBS. SK-BR-3 cells were cultured in McCoy's 5 A medium (Gibco) supplemented with 10% FBS. MCF 10A cells were cultured in specific epithelial culture medium (Procell Life Science & Technology Co., Ltd., Wuhan, China). Cells were cultured at 37 °C in a humidified incubator with 5% CO_2. All cell lines were confirmed to be mycoplasma-free, and their identity was verified using short tandem repeat (STR) profiling.

Plasmids UFL1, AKT1, AKT2 and AKT3 were cloned into pIRES-Flag-S, pLV.3-Flag, pLV.3-Flag-S, pLV.5-HA-S, pLV.6-GFP, pET28a and pGEX4T-1 vectors. Site-directed mutagenesis was employed to generate all mutants, with each construct confirmed by sequencing. In overexpression experiments, empty vectors served as the negative control.

https://doi.org/10.1038/s41467-026-68493-2

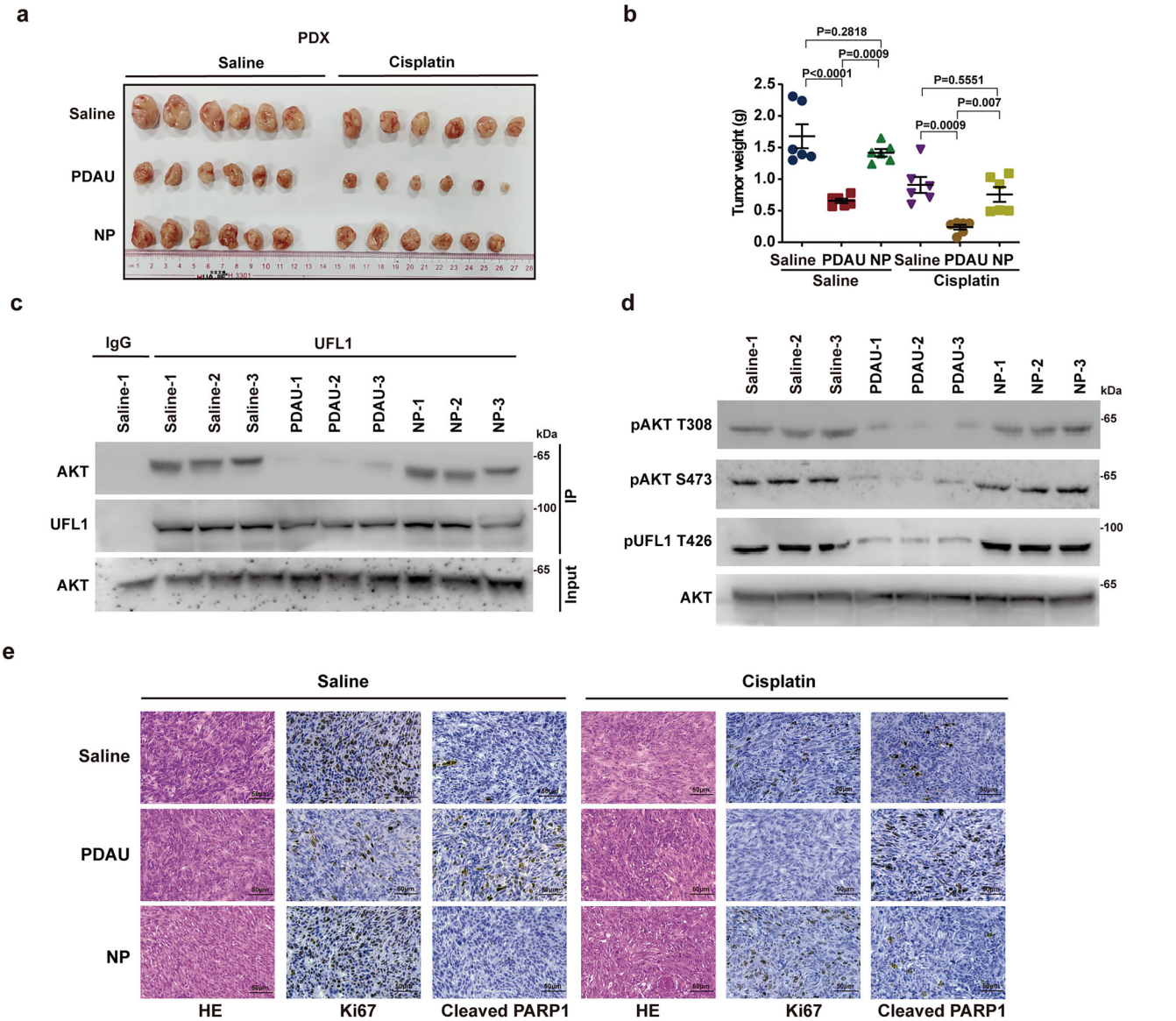

Fig. 7 | Disrupting the UFL1-AKT1 interaction by PDAU suppresses TNBC progression in vivo. a, **b** TNBC patient-derived xenografts (PDXs) were subcutaneously implanted into nude mice. Saline, PDAU or NP (15 mg/kg) was injected intraperitoneally every 2 days when tumor volume reached 100 mm^3. Mice were then treated with saline or cisplatin (5 mg/kg weekly, $n = 6$). Tumors were collected (**a**), and tumor weights were measured (**b**). Results represent the mean ± SD from six mice. **c** Cell lysates from PDXs treated with saline, PDAU or NP were subjected to immunoprecipitation with IgG, anti-UFL1 antibodies. The immunoprecipitates were blotted with the indicated antibodies. **d** Cell lysates from PDXs treated with saline, PDAU or NP were subjected to western blot with the indicated antibodies. **e** Representative images of H&E, Ki67 and cleaved PARP1 staining in xenograft models from (**a**). Scale bars, 50 μm. Data were analyzed by two-sided one-way ANOVA in (**b**). Source data are provided as a Source Data file.

Antibodies anti-Flag (F1804, dilution: 1:1000), anti-HA (H3663, dilution: 1:1000) and anti-β-actin (A1978, dilution: 1:5000) antibodies were purchased from Sigma-Aldrich. Anti-Myc (9E10, dilution: 1:1000) antibodies were purchased from Santa Cruz Biotechnology. Anti-Phospho-AKT Substrate (23C8D2, dilution: 1:1000), anti-p-AKT (T308) (13038S, dilution: 1:1000), anti-p-AKT (Ser473) (4060S, dilution: 1:1000), anti-Rictor (D16H9) (9476, dilution: 1:1000), anti-mTOR (7C10, dilution: 1:1000), anti-AKT (pan) antibody (2920S, dilution: 1:1000) and anti-GFP (4B10, dilution: 1:1000) antibodies were purchased from CST (Cell Signaling Technology). Anti-AKT1 (F0217, dilution: 1:1000), anti-AKT2 (F0218, dilution: 1:1000), anti-AKT3 (F0670, dilution: 1:1000), anti-PRAS40 (F0239, dilution: 1:1000) and anti-Phospho-PRAS40 (T246) (F0252, dilution: 1:1000) antibodies were purchased from Selleck. Anti-PHLPP1 (A9542, dilution: 1:500), anti-PP2A-B55α (A24261, dilution: 1:1000) and anti-PP2A-B56β (A14252, dilution: 1:1000) were purchased from ABclonal. Anti-UFM1 (ab109305, dilution: 1:1000) and anti-UFC1 (ab189251, dilution: 1:1000) antibodies were purchased from Abcam. Anti-UFL1 (A303-456A, dilution: 1:1000) antibodies were purchased from BETHYL. Anti-UFSP2 (16999-1-AP, dilution: 1:1000), anti-CDK5RAP3 (11007-1-AP, dilution: 1:1000) and anti-UFBP1 (21445-1-AP, dilution: 1:1000) antibodies were purchased from Proteintech. Anti-Phospho-UFL1 (T426) antibody (TP50605, dilution: 1:1000, custom antibody) was generated by immunizing rabbits with phospho-peptide, and then affinity-purified by Hangzhou HuaAn Biotechnology Co., Ltd. Light or heavy chain specific IPKine™ HRP (Abbkine Scientific Co.; A25012 and A25222) were used in the co-IP experiment.

RNA interference

In shRNA experiments, the shRNA targeting sequences for UFL1 shRNA #1 and #2 are 5′-GCTCTGGAACATGGGTTGATA-3′ and 5′-

https://doi.org/10.1038/s41467-026-68493-2

a

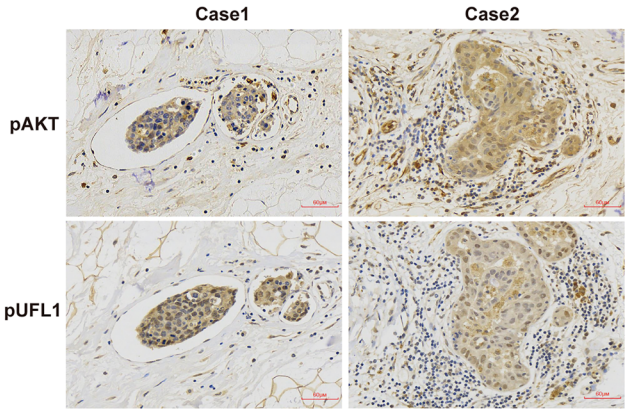

b

	pAKT High	pAKT Low	Total
pUFL1 High	35	0	35
pUFL1 Low	2	3	5

P=0.000115

c

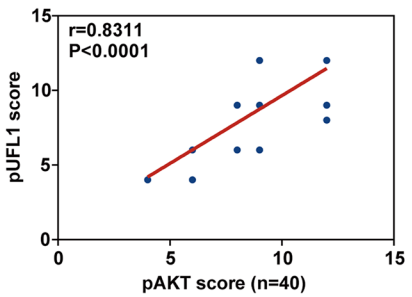

d

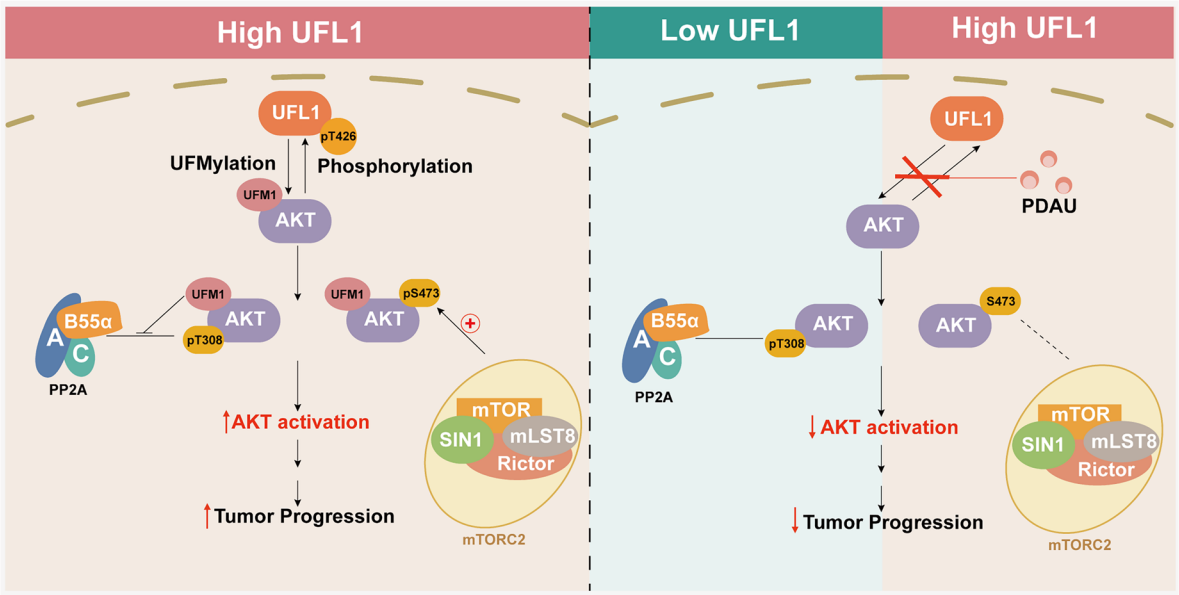

Fig. 8 | Correlations between pUFL1 and pAKT expression in TNBC. **a** Representative IHC staining of pUFL1 and pAKT in TNBC ($n = 40$). Scale bars, 60 μm. **b** Chi-square (χ^2) test analysis (two-sided) of pAKT and pUFL1 expression in TNBC ($n = 40$). **c** Pearson correlation analysis (two-sided) between pUFL1 and pAKT score in TNBC ($n = 40$), $r = 0.8311$, $P < 0.0001$. **d** Schematic representation of the experimental model of this study.

GAAACACTTCTGTGTCAGAAA-3′, respectively. The shRNA targeting sequences for AKT1/2 shRNA are 5′-CGCTACTACGCCATGAAGATC-3′, and the shRNA targeting sequences for AKT2/3 shRNA are 5′-ATGCTGGACAAAGATGGCCAC-3′. The shRNA targeting sequences for UFSP2 shRNA are 5′-GCTGAAGACCTGCAAGTTATT-3′. pLKO.1-scramble shRNA was used as a negative control with the sequence of CCTAAGGTTAAGTCGCCCTCG.

Western blotting analysis

Cell lysis was performed using NETN buffer (20 mM Tris-HCl, pH 8.0, 300 mM NaCl, 1 mM EDTA, 0.5% NP-40) containing 1× protease inhibitor cocktail (Roche), 10 mM β-glycerophosphate, 1 mM sodium orthovanadate, 10 mM sodium fluoride, and 1 mM PMSF. Following protein separation via SDS-PAGE and transfer to PVDF membranes, immunoblotting was conducted by incubating with primary and secondary antibodies.

CCK-8 assay

To assess cell viability, breast cancer cells were seeded in a 96-well plate at 2000 cells per well (100 μL medium with 10% FBS) in triplicate. After 72-h treatment with varying concentrations of cisplatin, tamoxifen, trastuzumab, paclitaxel, or doxorubicin, cell survival was measured using a Cell Counting Kit-8 (HY-K0301) by adding 15 μL of CCK-8 reagent and incubating for 2 h.

Cell proliferation assay

Breast cancer cells (2×10^4) were seeded in 6-well plates, and each group was in 6 wells. Cells for one of 6 wells were digested with 0.25% trypsin at 37 °C the next day. The cell pellets were collected by centrifugation (1100 g for 5 min), washed with PBS twice, re-suspended in PBS, and then counted in a microscope. Likewise, cells for the next 5 days are counted in a similar method.

Cell fractionation
Cell fractions were isolated using a Membrane and Cytosol Protein Extraction kit according to the manufacturer's instructions (Beyotime, Cat. No. P0033, Shanghai, China).

Immunoprecipitation
Cell lysates were prepared in NETN buffer for immunoprecipitation. Briefly, transfected HCC1806, MDA-MB-231, and HEK293T cells were incubated with anti-Flag affinity gel (Sigma) or S-agarose (Merck Millipore) at 4 °C for 4 h. Separately, HCC1806 and MDA-MB-231 cell lysates were subjected to immunoprecipitation by incubating overnight at 4 °C with the respective primary antibodies coupled to protein A/G beads (Thermo Scientific). Following five washes, the precipitated complexes were analyzed via western blotting.

Immunofluorescence staining
MDA-MB-231 cells grown on coverslips were processed for immunofluorescence. Following PBS washes, cells were fixed (4% formaldehyde, 20 min), permeabilized (0.1% Triton X-100, 5 min), and blocked (0.5% BSA, 1 h). Primary antibody incubation (anti-AKT1 and anti-UFL1, each at 1:200 dilution) was performed overnight at 4 °C, followed by secondary antibody incubation. Images were acquired with a confocal microscope to assess protein localization.

Glutathione S-transferase (GST) Pull-Down Assay
Target cDNAs were subcloned into pGEX4T-1 or pET28a expression vectors and subsequently transformed into the Escherichia coli strain BL21. Following overnight induction with 200 μM Isopropyl β-D-1-thiogalactopyranoside (IPTG) (Sigma, I6758-1G) at 18 °C, GST-tagged proteins, including GST alone, GST-AKT1, GST-AKT2, and GST-AKT3, were purified using Pierce Glutathione Agarose resin (Thermo Fisher Scientific). For in vitro binding assays, purified GST or GST-fusion proteins immobilized on the agarose beads were incubated with His-UFL1 for 4 h at 4 °C. Beads were washed four times, followed by western blotting.

UFMylation assay in vivo and in vitro
In vivo UFMylation assay. HEK293T cells were transiently transfected with AKT1 constructs along with the Myc- or HA-tagged UFMylation system components (UBA5, UFC1, UFL1, UFBP1, and UFM1 ΔC2). For detecting endogenous AKT1 UFMylation, MDA-MB-231 and HCC1806 cells were pretreated with 10 μM MG132 for 10 h prior to harvest. Cells were lysed 48 h post-transfection by boiling in buffer (150 mM Tris-HCl, pH 8, 5% SDS, 30% glycerol) for 10 min. Lysates were then diluted 20-fold with Buffer A (50 mM Tris-HCl, pH 8.0, 150 mM NaCl, 10 mM imidazole, 1% Triton X-100 or 0.5% NP-40, protease inhibitor cocktail, 2 mM NEM) and subjected to immunoprecipitation with specified antibodies, as previously described[10]. Immunoprecipitates were analyzed by Western blot to determine UFMylation levels.

In vitro UFMylation assay. Recombinant proteins were purified as described[7]. Briefly, GST-AKT1 was expressed in Escherichia coli strain BL21 and purified using glutathione agarose, while the His-tagged enzymes (UBA5, UFC1, UFL1, UFBP1, UFM1 ΔC2) were expressed similarly and purified with Ni-NTA agarose. For the reaction, purified proteins (each at 0.1 μM) were combined in assay buffer (50 mM HEPES pH 7.5, 5 mM ATP, 10 mM $MgCl_2$, 0.05% BSA) and incubated at 30 °C for 90 min. Reactions were terminated by adding SDS sample buffer containing 5% mercaptoethanol and boiling for 10 min.

In vivo and in vitro use of cell-penetrating peptides
Peptide corresponding to UFL1 amino acids 20–30 and its negative control corresponding to UFL1 amino acids 1–10 fused with a cell-penetrating peptide TAT (GRKKRRQRRRGG) were synthesized at Chinapeptides Co., Ltd (Shanghai, China).

The sequences of peptides used in this study were as follows: PDAU (GRKKRRQRRRGGFAEATQRLSER), NP (GRKKRRQRRRGGMAD AWEEIRR).

Cells were treated with 10 μM of the indicated peptides. Mice were injected with 15 mg/kg of the indicated peptides intraperitoneally every 2 days for 3 weeks.

Tumor xenograft assay in vivo
4–6-week-old BALB/c female nude mice were obtained from Jicui Yaokang Biotechnology Co., Ltd. (China) and randomly allocated to experimental groups. All animals were housed at 22–24 °C with 40-70% humidity under a 12/12-h light/dark cycle, with unrestricted access to food and water throughout the experiment. The xenograft experiment adhered to humane endpoint principles, with early euthanasia performed based on objective criteria including huddled posture, immobility, ruffled fur, failure to eat, hypothermia (colonic temperature <34 °C), or weight loss > 20%. Animals were euthanized immediately if they were unable to stand, displayed agonal breathing, severe muscular atrophy, severe ulceration, or uncontrolled bleeding. The maximum allowed subcutaneous tumor volume was 2000 mm^3, as authorized by the Committees on Animal Research and Ethics, and this limit was not exceeded during the experiments. HCC1806 cells (2×10^6) suspended in 100 μL PBS were subcutaneously injected into the flanks of female BALB/c-nude mice to establish xenografts. Tumor volume was assessed every two days via caliper measurements using the formula: V = a (short diameter)^2 × b (long diameter) ×0.5. Once tumors reached approximately 100 mm^3, mice were randomized into two groups ($n = 6$) and treated weekly with intraperitoneal injections of either saline or cisplatin (5 mg/kg). After six weeks, mice were euthanized, and tumors were excised and weighed.

TNBC Patient-derived xenograft (PDX) model. The TNBC PDXs were obtained from the tissue bank at Jinan University in accordance with approval from the Institutional Medical Ethics Committee (JNUKY-2023-0062) and with informed consent obtained from all donors. Specifically, PDXs were cut into pieces of $3 \times 3 \times 3$ mm^3 using sterile surgical instruments, and tumor blocks were inserted into the back of mice by inoculation needle. Tumor volumes were measured three times weekly by using a vernier caliper. Saline, PDAU or NP (15 mg/kg) was injected intraperitoneally every 2 days when tumor volume reached 100 mm^3. Mice were then treated with saline or cisplatin (5 mg/kg once a week), respectively ($n = 6$ per group). Mice were euthanized at the indicated time, and tumor weights were measured. Serum was collected from each mouse and used for liver (ALT, AST, ALP, DBIL, TBIL) and kidney function (CRE, UA) analyses by Servicebio, Wuhan, China. All animal experiments were performed in accordance with a protocol approved by the Institutional Animal Care and Use Committee (IACUC) in Jinan University (20241227-03).

Immunohistochemical staining
Tissue sections of TNBC patients were obtained from the tissue bank at Jinan University in accordance with the approval document of the Institutional Medical Ethics Committee (JNUKY-2023-0062). IHC assays were conducted on paraffin-embedded specimens using anti-pUFL1 or anti-pAKT antibodies, as previously described[61]. The final IHC score was determined by integrating two key parameters: the quantity score (reflecting the percentage of positively stained cells) and the staining intensity score. The quantity score was graded on a 0-4 scale: 0 = no immunostaining; 1 = 1–10% of cells showing positive staining; 2 = 11–50% of positive cells; 3 = 51–80% of positive cells; and 4 = ≥ 81% of positive cells. Staining intensity was assigned a score of 0 (negative), 1 (weak), 2 (moderate), or 3 (strong). For each tissue section, the composite IHC score was calculated by multiplying the intensity score by the quantity score, resulting in a total score ranging from 0 to 12. Immunoreactivity was further categorized based on this composite

score: 9–12 = strong immunoreactivity; 5–8 = moderate immunoreactivity; 1–4 = weak immunoreactivity; and 0 = negative immunoreactivity[62]. For downstream data analysis, samples with an IHC score of more than 6 were considered to be high, and less than 6 were considered to be low. We used GraphPad Prism to create a scatter plot with two quantitative variables, followed by linear correlation analysis to generate regression lines. The correlation between pUFL1 and pAKT was statistically analyzed using the χ^2-test and Pearson's correlation coefficient. For tumors harvested from animal experiments, histological and immunohistochemical analyses were performed. Briefly, tumor samples were fixed in 4% paraformaldehyde, paraffin-embedded, and sectioned at 5 μm thickness. Following dewaxing and dehydration, sections were subjected to hematoxylin and eosin (H&E) staining according to the manufacturer's protocol (E607318, Sangon Biotech), as well as immunohistochemical staining using antibodies against Ki67 (1:200 dilution) and cleaved PARP1 (1:200 dilution). All stained sections were visualized and imaged under an Olympus microscope.

Statistics and reproducibility

All data are analyzed by GraphPad Prism 5.0 software. Each experiment was performed at least three times, following the principle of repeatability. The experimental data represent the mean ± standard deviation (Mean ± SD). The differences between two groups of data were compared using a *t*-test, and the differences between multiple groups of data were compared using One-way ANOVA analysis of variance and Tukey's test: compare all pairs of columns. $P < 0.05$ is considered to be statistically significant.

Reporting summary

Further information on research design is available in the Nature Portfolio Reporting Summary linked to this article.

Data availability

All data generated or analyzed during this study are included within the article, Supplementary Information, the Source Data file, and the protein mass spectrometry raw data are available through the ProteomeXchange Consortium via the PRIDE partner repository with dataset identifiers PXD062168. Source data are provided with this paper.

References

1. Leon-Ferre, R. A. & Goetz, M. P. Advances in systemic therapies for triple-negative breast cancer. *BMJ (Clin. Res. ed.)* **381**, e071674 (2023).
2. Garrido-Castro, A. C., Lin, N. U. & Polyak, K. Insights into molecular classifications of triple-negative breast cancer: improving patient selection for treatment. *Cancer Discov.* **9**, 176–198 (2019).
3. Liu, J. et al. A critical role of DDRGK1 in endoplasmic reticulum homoeostasis via regulation of IRE1α stability. *Nat. Commun.* **8**, 14186 (2017).
4. Liang, J. R. et al. A genome-wide ER-phagy screen highlights key roles of mitochondrial metabolism and ER-resident UFMylation. *Cell* **180**, 1160–1177.e1120 (2020).
5. Tao, Y. et al. UFL1 promotes antiviral immune response by maintaining STING stability independent of UFMylation. *Cell Death Differ.* **30**, 16–26 (2023).
6. He, C. et al. UFL1 ablation in T cells suppresses PD-1 UFMylation to enhance anti-tumor immunity. *Mol. cell* **84**, 1120–1138.e1128 (2024).
7. Wang, Z. et al. MRE11 UFMylation promotes ATM activation. *Nucleic Acids Res.* **47**, 4124–4135 (2019).
8. Qin, B. et al. UFL1 promotes histone H4 ufmylation and ATM activation. *Nat. Commun.* **10**, 1242 (2019).
9. Yoo, H. M. et al. Modification of ASC1 by UFM1 is crucial for ERα transactivation and breast cancer development. *Mol. cell* **56**, 261–274 (2014).
10. Liu, J. et al. UFMylation maintains tumour suppressor p53 stability by antagonizing its ubiquitination. *Nat. Cell Biol.* **22**, 1056–1063 (2020).
11. Zhang, M. et al. RCAD/Ufl1, a Ufm1 E3 ligase, is essential for hematopoietic stem cell function and murine hematopoiesis. *Cell Death Differ.* **22**, 1922–1934 (2015).
12. Tatsumi, K. et al. The Ufm1-activating enzyme Uba5 is indispensable for erythroid differentiation in mice. *Nat. Commun.* **2**, 181 (2011).
13. Chen, F. et al. Loss of Ufl1/Ufbp1 in hepatocytes promotes liver pathological damage and carcinogenesis through activating mTOR signaling. *J. Exp. Clin. cancer Res.: CR* **42**, 110 (2023).
14. Yoo, H. M., Park, J. H., Kim, J. Y. & Chung, C. H. Modification of ERα by UFM1 increases its stability and transactivity for breast cancer development. *Mol. cells* **45**, 425–434 (2022).
15. Lauring, J., Park, B. H. & Wolff, A. C. The phosphoinositide-3-kinase-Akt-mTOR pathway as a therapeutic target in breast cancer. *J. Natl. Compr. Canc. Netw.* **11**, 670–678 (2013).
16. Hua, H. et al. Targeting Akt in cancer for precision therapy. *J. Hematol. Oncol.* **14**, 128 (2021).
17. Bellacosa, A. et al. Akt activation by growth factors is a multiple-step process: the role of the PH domain. *Oncogene* **17**, 313–325 (1998).
18. Higuchi, M., Onishi, K., Kikuchi, C. & Gotoh, Y. Scaffolding function of PAK in the PDK1-Akt pathway. *Nat. Cell Biol.* **10**, 1356–1364 (2008).
19. Sarbassov, D. D., Guertin, D. A., Ali, S. M. & Sabatini, D. M. Phosphorylation and regulation of Akt/PKB by the rictor-mTOR complex. *Sci. (N. Y., N. Y.)* **307**, 1098–1101 (2005).
20. Manning, B. D. & Toker, A. AKT/PKB signaling: navigating the network. *Cell* **169**, 381–405 (2017).
21. Basu, S., Totty, N. F., Irwin, M. S., Sudol, M. & Downward, J. Akt phosphorylates the Yes-associated protein, YAP, to induce interaction with 14-3-3 and attenuation of p73-mediated apoptosis. *Mol. cell* **11**, 11–23 (2003).
22. Brognard, J., Sierecki, E., Gao, T. & Newton, A. C. PHLPP and a second isoform, PHLPP2, differentially attenuate the amplitude of Akt signaling by regulating distinct Akt isoforms. *Mol. cell* **25**, 917–931 (2007).
23. Gao, T., Furnari, F. & Newton, A. C. PHLPP: a phosphatase that directly dephosphorylates Akt, promotes apoptosis, and suppresses tumor growth. *Mol. cell* **18**, 13–24 (2005).
24. Padmanabhan, S. et al. A PP2A regulatory subunit regulates C. elegans insulin/IGF-1 signaling by modulating AKT-1 phosphorylation. *Cell* **136**, 939–951 (2009).
25. Ruvolo, P. P. et al. Low expression of PP2A regulatory subunit B55α is associated with T308 phosphorylation of AKT and shorter complete remission duration in acute myeloid leukemia patients. *Leukemia* **25**, 1711–1717 (2011).
26. Song, M. S., Salmena, L. & Pandolfi, P. P. The functions and regulation of the PTEN tumour suppressor. *Nat. Rev. Mol. cell Biol.* **13**, 283–296 (2012).
27. Qin, S. et al. SHIP-1 regulates phagocytosis and M2 polarization through the PI3K/Akt-STAT5-trib1 circuit in pseudomonas aeruginosa infection. *Front. Immunol.* **11**, 307 (2020).
28. Sementino, E., Hassan, D., Bellacosa, A. & Testa, J. R. AKT and the Hallmarks of Cancer. *Cancer Res* **84**, 4126–4139 (2024).
29. Miricescu, D. et al. PI3K/AKT/mTOR signaling pathway in breast cancer: from molecular landscape to clinical aspects. *Int. J. Mol. Sci.* **22**, 173 (2020).
30. Jin, Y. et al. Activation of PI3K/AKT pathway is a potential mechanism of treatment resistance in small cell lung cancer. *Clin. Cancer Res* **28**, 526–539 (2022).
31. He, Y. et al. Targeting PI3K/Akt signal transduction for cancer therapy. *Signal Transduct. Target. Ther.* **6**, 425 (2021).
32. Khan, M. A., Jain, V. K., Rizwanullah, M., Ahmad, J. & Jain, K. PI3K/AKT/mTOR pathway inhibitors in triple-negative breast cancer: a

review on drug discovery and future challenges. *Drug Discov. Today* **24**, 2181–2191 (2019).
33. Shi, Z. et al. Functional mapping of AKT signaling and biomarkers of response from the FAIRLANE trial of neoadjuvant ipatasertib plus paclitaxel for triple-negative breast cancer. *Clin. Cancer Res* **28**, 993–1003 (2022).
34. Shah, S. P. et al. The clonal and mutational evolution spectrum of primary triple-negative breast cancers. *Nature* **486**, 395–399 (2012).
35. Comprehensive molecular portraits of human breast tumours. *Nature* **490**, 61-70 (2012).
36. Pascual, J. & Turner, N. C. Targeting the PI3-kinase pathway in triple-negative breast cancer. *Ann. Oncol.* **30**, 1051–1060 (2019).
37. Sánchez-Muñoz, A. et al. Lack of evidence for KRAS oncogenic mutations in triple-negative breast cancer. *BMC Cancer* **10**, 136 (2010).
38. Wang, X., Lv, X., Ma, J. & Xu, G. UFMylation: an integral post-translational modification for the regulation of proteostasis and cellular functions. *Pharmacol. Ther.* **260**, 108680 (2024).
39. Song, M., Bode, A. M., Dong, Z. & Lee, M. H. AKT as a therapeutic target for cancer. *Cancer Res* **79**, 1019–1031 (2019).
40. Knudsen, J. R. et al. Growth factor-dependent and -independent activation of mTORC2. *Trends Endocrinol. Metab.: TEM* **31**, 13–24 (2020).
41. Kuo, Y. C. et al. Regulation of phosphorylation of Thr-308 of Akt, cell proliferation, and survival by the B55alpha regulatory subunit targeting of the protein phosphatase 2A holoenzyme to Akt. *J. Biol. Chem.* **283**, 1882–1892 (2008).
42. Itoh, Y. et al. PDK1-Akt pathway regulates radial neuronal migration and microtubules in the developing mouse neocortex. *Proc. Natl. Acad. Sci. USA* **113**, E2955–2964 (2016).
43. Bu, L. et al. PTEN suppresses tumorigenesis by directly dephosphorylating Akt. *Signal Transduct. Target. Ther.* **6**, 262 (2021).
44. DaRosa, P. A. et al. UFM1 E3 ligase promotes recycling of 60S ribosomal subunits from the ER. *Nature* **627**, 445–452 (2024).
45. Zhao, K. et al. Akt-phosphorylated UFL1 UFMylates ArpC4 to promote metastasis. *Nat. Struct. Mol. Biol.* **32**, 1528–1541 (2025).
46. Zorko, M., Jones, S. & Langel, Ü Cell-penetrating peptides in protein mimicry and cancer therapeutics. *Adv. drug Deliv. Rev.* **180**, 114044 (2022).
47. Guidotti, G., Brambilla, L. & Rossi, D. Cell-penetrating peptides: from basic research to clinics. *Trends Pharmacol. Sci.* **38**, 406–424 (2017).
48. Risso, G., Blaustein, M., Pozzi, B., Mammi, P. & Srebrow, A. Akt/PKB: one kinase, many modifications. *Biochem. J.* **468**, 203–214 (2015).
49. Yang, W. L. et al. The E3 ligase TRAF6 regulates Akt ubiquitination and activation. *Sci. (N. Y., N. Y.)* **325**, 1134–1138 (2009).
50. Chan, C. H. et al. The Skp2-SCF E3 ligase regulates Akt ubiquitination, glycolysis, herceptin sensitivity, and tumorigenesis. *Cell* **149**, 1098–1111 (2012).
51. Zhou, J. et al. Dysregulation of PD-L1 by UFMylation imparts tumor immune evasion and identified as a potential therapeutic target. *Proc. Natl. Acad. Sci. USA* **120**, e2215732120 (2023).
52. Sun, N. et al. A novel nuclear RNA HSD52 scaffolding NONO/SFPQ complex modulates DNA damage repair to facilitate temozolomide resistance. *Neuro-oncol.* **27**, 963–978 (2024).
53. Huang, J. et al. Targeting the PI3K/AKT/mTOR signaling pathway in the treatment of human diseases: current status, trends, and solutions. *J. Med Chem.* **65**, 16033–16061 (2022).
54. Okuzumi, T. et al. Inhibitor hijacking of Akt activation. *Nat. Chem. Biol.* **5**, 484–493 (2009).
55. Burstein, H. J., DeMichele, A., Fallowfield, L., Somerfield, M. R. & Henry, N. L. Endocrine and targeted therapy for hormone receptor-positive, human epidermal growth factor receptor 2-negative metastatic breast cancer-capivasertib-fulvestrant: ASCO rapid recommendation update. *J. Clin. Oncol.: Off. J. Am. Soc. Clin. Oncol.* **42**, 1450–1453 (2024).
56. Howell, S. J. et al. Fulvestrant plus capivasertib versus placebo after relapse or progression on an aromatase inhibitor in metastatic, oestrogen receptor-positive, HER2-negative breast cancer (FAKTION): overall survival, updated progression-free survival, and expanded biomarker analysis from a randomised, phase 2 trial. *Lancet Oncol.* **23**, 851–864 (2022).
57. Chu, A., Hakami-Majd, N. & Whall, J. O. Acute hyperglycemic hyperosmolar syndrome associated with capivasertib, a new, oral targeted therapy for advanced breast cancer. *Am. J. Emerg. Med.* **88**, 273.e275–273.e277 (2025).
58. Xiao, M. C. et al. TRIB3-TRIM8 complex drives NAFLD progression by regulating HNF4α stability. *J. Hepatol.* **80**, 778–791 (2024).
59. Zhang, Y. et al. BTApep-TAT peptide inhibits ADP-ribosylation of BORIS to induce DNA damage in cancer. *Mol. Cancer* **21**, 158 (2022).
60. Fang, P., Pang, W. K., Xuan, S., Chan, W. L. & Leung, K. C. Recent advances in peptide macrocyclization strategies. *Chem. Soc. Rev.* **53**, 11725–11771 (2024).
61. Guan, T. et al. Phosphorylation of USP29 by CDK1 Governs TWIST1 Stability and Oncogenic Functions. *Adv. Sci.* **10**, e2205873 (2023).
62. Luo, K. et al. USP49 negatively regulates tumorigenesis and chemoresistance through FKBP51-AKT signaling. *Embo J.* **36**, 1434–1446 (2017).

Acknowledgments

We are grateful to Professor Ping Hu of Jinan University for providing essential support with the pharmacokinetic research. This study was supported by by Science and Technology Project in Guangzhou (202102070001 TL), Science and Technology Project of Guangdong Province (2023A0505050149 TL), National Natural Science Foundation of China (82473109 TL and 82404654 YW), Guangdong Major Project of Basic and Applied Basic Research (2023B0303000026 TL), Guangdong Basic and Applied Basic Research Foundation (2024A1515013266 TL, 2025A1515012357 TL and 2024B1515040007 TL) and China Postdoctoral Science Foundation (2024M750581 YW).

Author contributions

T.L. conceived the study and designed the experiments. X.Y. performed most experiments with assistance from Y.W., X.M., S.Q., Y.L., and J.C. T.L., X.Y., and Y.W. wrote the manuscript, and H.Z., C.G., and R.C. helped revise it. T.L., C.G., and R.C. guided and supervised the study. All authors discussed and commented on the manuscript.

Competing interests

The authors declare no competing interests.

Additional information

Supplementary information The online version contains supplementary material available at https://doi.org/10.1038/s41467-026-68493-2.

Correspondence and requests for materials should be addressed to Tongzheng Liu.

Peer review information *Nature Communications* thanks the anonymous reviewer(s) for their contribution to the peer review of this work. A peer review file is available.